The Astrophysical Journal, 819:127 (5pp), 2016 March 10 doi:10.3847/0004-637X/819/2/127

MASS–RADIUS RELATION FOR ROCKY PLANETS BASED ON PREM

Li Zeng[1], Dimitar D. Sasselov[2], and Stein B. Jacobsen[1]
[1] Department of Earth and Planetary Sciences, Harvard University, Cambridge, MA 02138, USA; astrozeng@gmail.com, jacobsen@neodymium.harvard.edu
[2] Astronomy Department, Harvard University, Cambridge, MA 02138, USA; dsasselov@cfa.harvard.edu
Received 2015 February 25; accepted 2016 February 2; published 2016 March 8

ABSTRACT

Several small dense exoplanets are now known, inviting comparisons to Earth and Venus. Such comparisons require translating their masses and sizes to composition models of evolved multi-layer interior planets. Such theoretical models rely on our understanding of the Earth's interior, as well as independently derived equations of state, but so far have not involved direct extrapolations from Earth's seismic model: the Preliminary Reference Earth Model (PREM). To facilitate more detailed compositional comparisons between small exoplanets and the Earth, we derive here a semi-empirical mass–radius relation for two-layer rocky planets based on PREM, $\frac{R}{R_\oplus} = (1.07 - 0.21 \cdot \mathrm{CMF}) \cdot \left(\frac{M}{M_\oplus}\right)^{1/3.7}$, where CMF stands for core mass fraction. It is applicable to $1 \sim 8\ M_\oplus$ and a CMF of $0.0 \sim 0.4$. Applying this formula to Earth and Venus and several known small exoplanets with radii and masses measured to better than ~30% precision gives a CMF fit of 0.26 ± 0.07.

Key words: planets and satellites: composition – planets and satellites: general – planets and satellites: interiors

Supporting material: machine-readable table

1. INTRODUCTION

A first step in deriving the compositional diversity of small rocky planets was accomplished recently by (Dressing et al. 2015), who added Kepler-93b to the list of a dozen or so small exoplanets with radii and masses measured to better than ~30% precision. With exquisite sizes (mostly from *Kepler* light curves) and huge follow-up efforts (Batalha et al. 2011; Hatzes et al. 2011; Carter et al. 2012; Ballard et al. 2014; Pepe et al. 2013; Berta-Thompson et al. 2015; Dressing et al. 2015) the mass–radius diagram is finally amenable to some detailed comparisons with theory in the 1–10 $M_\oplus$ range. Closer to the mass and size of Earth, the rocky planets known to date seem to exhibit an unexpectedly tight compositional correlation. Is this correlation really shared with Earth and Venus? If so, to what level of precision and under what assumptions? To begin answering such questions we must first acknowledge that models of the interior structure and composition of rocky exoplanets in the super-Earth domain are based largely on experience (and extrapolations) from the models of the rocky solar system planets, and mostly the Earth (Valencia et al. 2006, 2007a, 2007b; Fortney et al. 2007; Seager et al. 2007; Zeng & Seager 2008; Grasset et al. 2009; Zeng & Sasselov 2013). Here, instead of using simple shell models based on equations of state (EOSs) of minerals and metals, we take a different approach and derive semi-empirical EOSs based on the well-constrained seismic model of the Earth.

2. EQUATION OF STATE (EOS)

On one hand, in several previous models of solid exoplanets (Seager et al. 2007; Zeng & Seager 2008; Zeng & Sasselov 2013), the cores and mantles were modeled as pure ϵ-Fe-solid and Mg-perovskite/post-perovskite, respectively. On the other hand, we know the actual density variation inside Earth through measurements of seismic wave velocities. This seismically derived density model is widely known as the Preliminary Reference Earth Model (PREM) (Dziewonski & Anderson 1981). The differences between the two approaches, primarily (1) the liquid outer core is less dense than pure ϵ-Fe-solid and (2) the upper mantle is less dense than the extrapolation of the lower mantle, can cause differences in the mass–radius relations derived.

There are several assumptions when we extrapolate PREM. We assume that the upper mantle to lower mantle phase transition occurs at the same pressure as the Earth's interior. It is a pressure-driven phase transition, so the temperature effect is secondary and thus ignored.

The Thomas–Fermi–Dirac Model modified with correlation energy (Salpeter & Zapolsky 1967) (abbreviated as TFD) serves as a lower bound for the density of material considered. Any properly behaving EOS should asymptotically approach a TFD above ~1 TPa, as the electron degeneracy pressure dominates while the detailed chemical and crystal structures of the material become less important at such high pressures.

We will show that the Birch–Murnaghan second-order EOS (abbreviated as BM2) (Birch 1952) provides a fairly decent description of how material is compressed in the Earth's interior for both the core (good up to 12 TPa where it asymptotically approaches TFD) and the mantle (good up to 3.5 TPa where it asymptotically approaches TFD). Those pressures roughly correspond to the central pressure and core–mantle boundary pressure, respectively, of a 30 $M_\oplus$ rocky planet where the CMF = 0.3.

$$P = \frac{3}{2} \cdot K_0 \left[\left(\frac{\rho}{\rho_0}\right)^{\frac{7}{3}} - \left(\frac{\rho}{\rho_0}\right)^{\frac{5}{3}} \right]. \quad (1)$$

The fit to the lower mantle, the outer core, and the inner core PREM gives:

1. Lower mantle: $\rho_0 = 3.98$ g/cc, $K_0 = 206$ GPa, error ~1% in ρ.
2. Outer core: $\rho_0 = 7.05$ g/cc, $K_0 = 201$ GPa, error ~1% in ρ.
3. Inner core: $\rho_0 = 7.85$ g/cc, $K_0 = 255$ GPa, error ~0.01% in ρ.

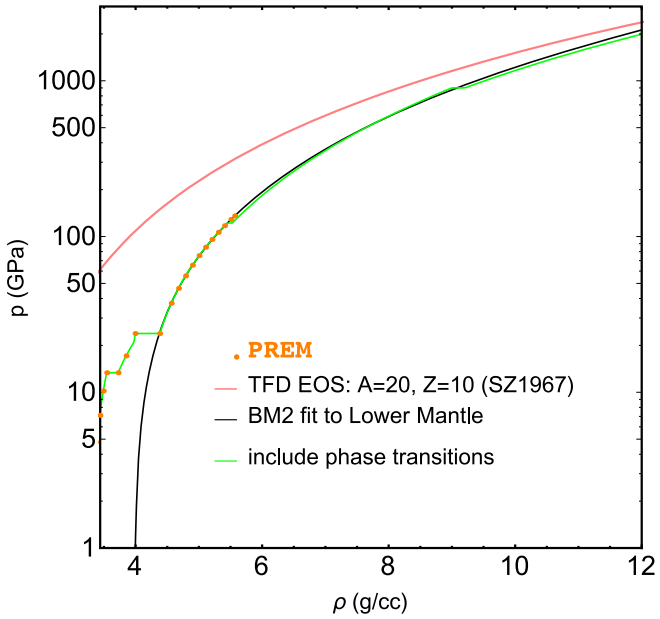

Figure 1. Orange points: PREM density of the Earth's mantle, excerpt from Appendix G of (Stacey & Davis 2008). Pink curve: TFD for $A = 20$ and $Z = 10$. Black curve: BM2 fit to lower-mantle PREM ($\rho_0 = 3.98$ g/cc, $K_0 = 206$ GPa). Green curve: includes lower-mantle phase transitions and pv-ppv phase transition at 122 GPa (Spera et al. 2006; Caracas & Cohen 2008; Zeng & Sasselov 2013) and further dissociation of ppv at 0.9 and 2.1 TPa (Umemoto & Wentzcovitch 2011; Wu et al. 2011).

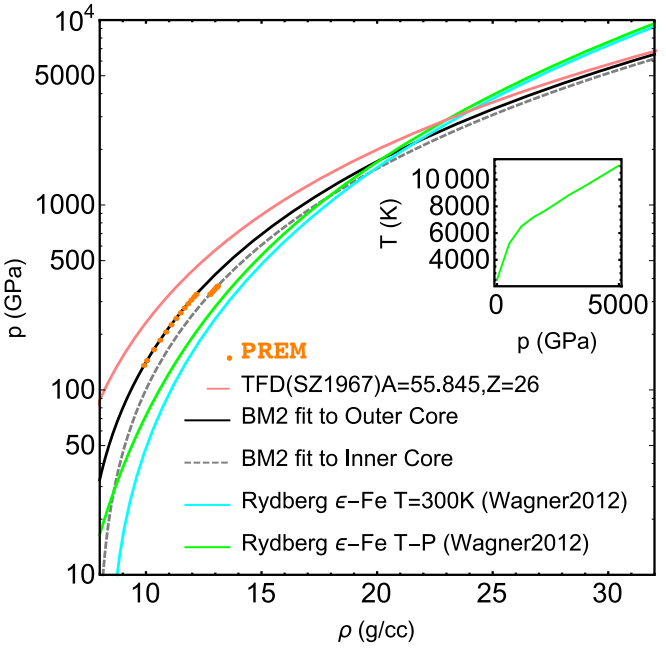

Figure 2. Orange points: PREM density of Earth's core, excerpt from Appendix G of (Stacey & Davis 2008). Pink curve: TFD of iron ($A = 55.845$ and $Z = 26$). Black curve: BM2 fit to outer-core PREM ($\rho_0 = 7.05$ g/cc, $K_0 = 201$ GPa). Gray dashed curve: BM2 fit to inner-core PREM ($\rho_0 = 7.85$ g/cc, $K_0 = 255$ GPa). Cyan curve: Rydberg ϵ-Fe EOS at 300 K isotherm according to (Dewaele et al. 2006). Green curve: Rydberg ϵ-Fe EOS (Dewaele et al. 2006) with T-P profile (small inlet plot) of rocky planet core interpolated from Wagner et al. (2012).

The uncertainties of the fit are similar to the intrinsic uncertainty of the PREM in ρ of $\sim$1% (see Ricolleau et al. 2009 and Ritsema et al. 2011 and Figure 3 of Huang et al. 2011).

2.1. PREM-extrapolated EOS for Mantle

Inside Earth, the density jump from the upper mantle to the lower mantle is 10% from 4 g/cc to 4.4 g/cc at 23.83 GPa. Earth's upper mantle consists of complex phases of Mg-silicates, including various polymorphs of olivine: (α) olivine, (β) wadsleyite, and (γ) ringwoodite (Bina 2003). The upper mantle to lower mantle transition occurs at a 670 km depth in the Earth (about 10.5% Earth radius). For more massive planets like Kepler-93b, this transition occurs at shallower depth ($\sim$3% radius of Kepler-93b) for the same pressure.

Figure 1 shows the comparison of different EOS of Mg-silicates.

Interestingly, the TFD beyond 1 TPa for MgO, SiO_2, $MgSiO_3$, and Mg_2SiO_4 are almost identical because they all have an average atomic weight of $A = 20$ and an average atomic charge of $Z = 10$. This coincidence simplifies the EOS of Mg-silicates, as it indicates that Mg/Si ratio does not matter toward the high-pressure end; it only matters toward the low-pressure end, which is captured in our EOS by using the PREM density variation in the upper-mantle pressure range.

According to Figure 1, except for the prominent density jump of 10% at the upper-lower mantle boundary, the other high-pressure phase transitions are only $\sim$1% level in density, and thus insignificant in mass–radius calculation (Unterborn et al. 2015). Therefore, in this paper we adopt the EOS of Mg-silicates mantle as follows:

1. 0 GPa–23.83 GPa: linear interpolation of the lower mantle density according to Appendix G of (Stacey & Davis 2008), which is taken from PREM. i.e., follow the green curve in Figure 1.
2. 23.83 GPa–3.5 TPa: BM2 EOS with $\rho_0 = 3.98$ g/cc, $K_0 = 206$ GPa, (error $\sim$1% in density). i.e., follow the black curve in Figure 1.
3. >3.5 TPa: TFD EOS of $MgSiO_3$ calculated using method in (Salpeter & Zapolsky 1967). i.e., follow the pink curve in Figure 1.

2.2. PREM-extrapolated EOS for Core

Figure 2 shows the comparison of different EOS of the Core.

In the Earth, the density jump from liquid outer core to solid inner core is 5% from 12.2 g/cc to 12.8 g/cc at 328.85 GPa. The Rydberg EOS of the pure solid ϵ-Fe phase, which is experimentally determined from static compression up to 205 GPa (Dewaele et al. 2006; Wagner et al. 2012), is too high of a density (cyan curve in Figure 2) in the pressure region relevant to Earth, even including the temperature effect (green curve in Figure 2), even for the solid inner core. This is likely due to the presence of several weight percent of one or more light elements (McDonough 2014, pp. 559–577). The lighter elements could be S, Si, O, C, or a combination of them (Anderson & Ahrens 1994; Poirier 1994; Stixrude et al. 1997; Alfè et al. 2002; Badro et al. 2007; Fischer et al. 2012), but no agreement is reached as to which of these elements are the most important. The Rydberg EOS with or without temperature behaves poorly for extrapolation above $\sim$1 TPa as it overshoots and crosses over the TFD EOS, which serves as a lower bound for the density of Fe.

As such, we choose to only extrapolate the liquid outer core BM2 EOS to higher pressure until it asymptotically approaches

the TFD EOS. The solid inner core is likely a secondary feature resulting from the crystallization of the liquid core. It currently comprises only a small fraction (≈3%) of the total mass of the Earth, and in more massive planets, which is the focus of this study, a solid inner core may not exist at all due to a higher heat content and a slower cooling rate. BM2 EOS behaves nicely as it asymptotically approaches the TFD EOS at very high pressure (∼12 TPa).

Therefore, in this paper we adopt the EOS of Fe core as follows:

1. 0 GPa–12 TPa: BM2 EOS with $\rho_0 = 7.05$ g/cc, $K_0 =$ 201 GPa, (error ∼1% in density). i.e., follow the black curve in Figure 2.
2. 12 TPa: TFD EOS of Fe ($A = 55.845$ and $Z = 26$) calculated using method in (Salpeter & Zapolsky 1967). i.e., follow the pink curve in Figure 2.

3. MASS–RADIUS RELATION

Dressing et al. (2015) point out a tight mass–radius relation of solid exoplanets between 2 and 5 $M_\oplus$ from the comparison of Earth, Venus, and several dense exoplanets by using the mass–radius contours described in (Zeng & Sasselov 2013). However, Dressing et al. (2015) have a CMF fit of 17%, much lower than that of Earth or Venus. Here we show that using the PREM-extrapolated EOS renders a better fit of CMF in agreement with that of Earth and Venus (See Figure 3).

There might be a selection bias toward higher-density planets by selecting only those with better than ∼30% mass measurement accuracy. However, as already pointed out by Dressing et al. (2015), the low-mass planets with very low densities like Kepler-11b and Kepler-138d, do not detract from the conclusion that all the rocky analogs of the Earth obey a single mass–radius relation. The degree to which this is true will be tested by more precise mass measurements.

The planets in Figure 3 are tabulated in Table 1.

The mass–radius curves in Figure 3 are tabulated in Table 2.

3.1. Mass–Radius Formula Fitting for Rocky Planets

The CMF-dependent mass–radius relation of rocky planets can be fit to the following formula (for $0 \leqslant \mathrm{CMF} \leqslant 0.4$, $1M_\oplus \leqslant M \leqslant 8\,M_\oplus$). It agrees with the actual mass–radius curves in Figure 3 within ∼0.01 $R_\oplus$ in radius. If we use it to calculate the CMF, it gives an uncertainty of ∼0.02.

$$\left(\frac{R}{R_\oplus}\right) = (1.07 - 0.21 \cdot \mathrm{CMF})\left(\frac{M}{M_\oplus}\right)^{1/3.7}. \quad (2)$$

Equation (2) can be inverted to solve for CMF, given the mass and radius.

$$\mathrm{CMF} = \frac{1}{0.21}\left[1.07 - \left(\frac{R}{R_\oplus}\right)\Big/\left(\frac{M}{M_\oplus}\right)^{1/3.7}\right]. \quad (3)$$

For comparison, this semi-empirical mass–radius formula is in agreement with the mass–radius relation of super-Earths presented in Valencia et al. (2006), which is a scaling law of $R \propto M^{0.267-0.272}$. This new formula takes one step further to articulate the dependence on the CMF, which is useful in differentiating among rocky planets with different CMFs (i.e., compositions).

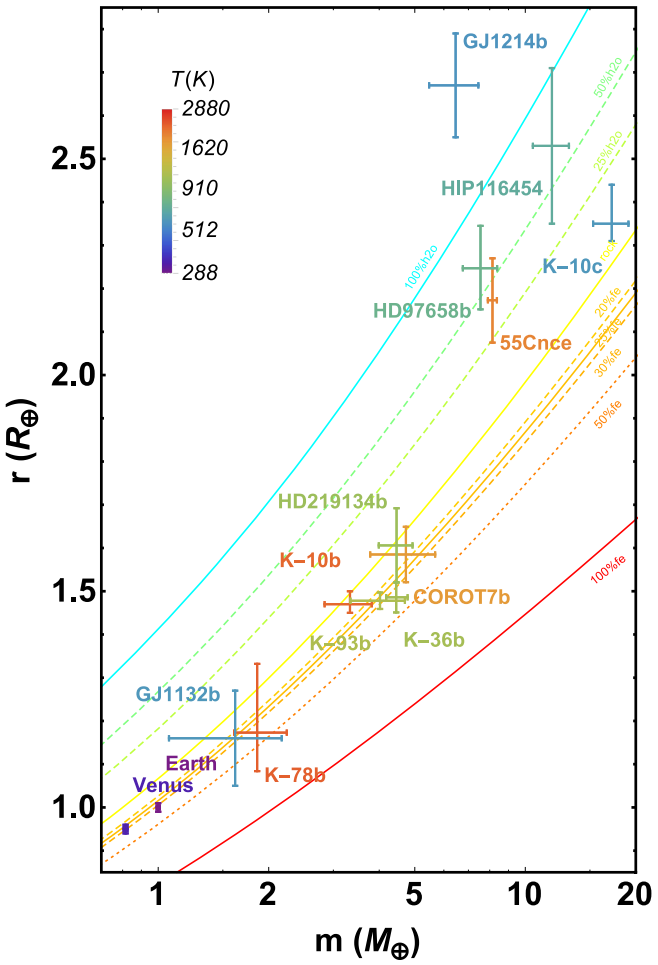

Figure 3. Mass-radius curves with planets color-coded by their surface temperatures (calculated from the stellar flux they receive, assuming similar bond albedo as the Earth (≈0.3) and perfect heat redistribution). (Charbonneau et al. 2009; Cochran et al. 2011; Winn et al. 2011; Carter et al. 2012; Ballard et al. 2014; Dragomir et al. 2013; Pepe et al. 2013; Barros et al. 2014; Dumusque et al. 2014; Haywood et al. 2014; Nelson et al. 2014; Berta-Thompson et al. 2015; Dressing et al. 2015; Motalebi et al. 2015; Vanderburg et al. 2015).

For Earth, $\mathrm{CMF}_\oplus = \frac{1}{0.21}[1.07 - (1)/(1)^{1/3.7}] = 0.07/0.21 = 0.33$. For Kepler-93b, $\mathrm{CMF}_{\mathrm{K93b}} = \frac{1}{0.21}[1.07 - (1.478)/(4.02)^{1/3.7}] = 0.26$. The uncertainties ($\delta$CMF) in CMF resulting from the uncertainties in mass and radius can be derived from Equation (3):

$$|\delta\mathrm{CMF}| \approx 5 \times \sqrt{\left|\frac{\delta r}{r}\right|^2 + \left(\frac{1}{3.7}\right)^2 \left|\frac{\delta m}{m}\right|^2}. \quad (4)$$

To tell a 20% core mass apart from a 30% core mass, the radius needs to be measured to better than a 2% level, or equivalently, mass to a 6% level. For Kepler-93b, $\left|\frac{\delta r}{r}\right| = \frac{0.019}{1.478} = 0.013$ and $\left|\frac{\delta m}{m}\right| = \frac{0.68}{4.02} = 0.17$, so $|\delta\mathrm{CMF}| = 0.2$. Therefore, $\mathrm{CMF}_{\mathrm{K93b}} = 0.26 \pm 0.2$. Table 1, column 4, lists the CMF estimates of these exoplanets.

Assuming this population of dense exoplanets follows the same CMF distribution, we then apply a weighted least-square fit to Table 1.

Table 1
CMF of Planets

Planet	$M(M_\oplus)$	$R(R_\oplus)$	CMF
Earth[a]	1	1	0.325 ± 0.001
Venus[a]	0.815	0.9499	0.31 ± 0.01
K-10b	3.33 ± 0.49 (Dumusque et al. 2014)	$1.47^{+0.03}_{-0.02}$ (Dumusque et al. 2014)	0.04 ± 0.2
K-36b	$4.45^{+0.33}_{-0.27}$ (Carter et al. 2012)	1.486 ± 0.035 (Carter et al. 2012)	0.37 ± 0.14
K-78b	$1.86^{+0.38}_{-0.25}$ (Pepe et al. 2013)	$1.173^{+0.159}_{-0.089}$ (Pepe et al. 2013)	$0.37^{+0.3}_{-0.5}$
K-93b	4.02 ± 0.68 (Dressing et al. 2015)	1.478 ± 0.019 (Ballard et al. 2014)	0.26 ± 0.2
COROT-7b	5.74 ± 0.86 (Haywood et al. 2014)	1.585 ± 0.064 (Barros et al. 2014)	0.14 ± 0.3
HD219134b	4.46 ± 0.47 (Motalebi et al. 2015)	1.606 ± 0.086 (Motalebi et al. 2015)	0.0 ± 0.3
GJ1132b	1.62 ± 0.55 (Berta-Thompson et al. 2015)	1.16 ± 0.11 (Berta-Thompson et al. 2015)	0.25 ± 0.5

Note.
[a] In the calculation we treat the errors in the CMF of Earth and Venus as ± 0.2, comparable to the errors for exoplanets considered here, so as not to bias the fit.

Table 2
Mass–Radius Table

	100%fe	50%fe	30%fe	25%fe	20%fe	Rock	25%h2o	50%h2o	100%h2o
$M(M_\oplus)$[a]	$R(R_\oplus)$[b]	$R(R_\oplus)$	$R(R_\oplus)$	$R(R_\oplus)$	$R(R_\oplus)$	$R(R_\oplus)$	$R(R_\oplus)$	$R(R_\oplus)$	$R(R_\oplus)$
0.125	0.445	0.523	0.547	0.553	0.558	0.58	0.649	0.697	0.776
0.25	0.55	0.645	0.672	0.679	0.685	0.711	0.793	0.851	0.952
0.5	0.676	0.789	0.823	0.832	0.84	0.872	0.969	1.039	1.163
1	0.823	0.961	1.005	1.016	1.026	1.067	1.182	1.27	1.41
2	0.99	1.164	1.22	1.23	1.25	1.3	1.44	1.54	1.71
4	1.176	1.4	1.47	1.49	1.5	1.57	1.74	1.85	2.05
8	1.38	1.66	1.75	1.77	1.79	1.88	2.07	2.21	2.45
16	1.59	1.94	2.06	2.08	2.11	2.22	2.45	2.61	2.9
32	1.82	2.25	2.38	2.42	2.45	2.58	2.85	3.04	3.36

Notes.
[a] Mass in Earth Mass ($M_\oplus = 5.9742 \times 10^{24}$ kg).
[b] Radius in Earth Radius ($R_\oplus = 6.371 \times 10^6$ m).
(This table is available in machine-readable form.)

Denote the weighted average of the CMF as $\overline{\mathrm{CMF}}$.

$$\overline{\mathrm{CMF}} = \frac{\sum_i \left(\frac{\mathrm{CMF}}{\delta \mathrm{CMF}^2} \right)}{\sum_i \left(\frac{1}{\delta \mathrm{CMF}^2} \right)} \tag{5}$$

Denote the standard deviation of the CMF as σCMF.

$$\sigma \mathrm{CMF} = \sqrt{1 \Big/ \left(\sum_i \frac{1}{\delta \mathrm{CMF}^2} \right)} \tag{6}$$

The result is $\overline{\mathrm{CMF}} = 0.26$ and $\sigma \mathrm{CMF} = 0.07$, indicating Earth-like composition (CMF $\sim$ 0.3) carries on up to at least $\sim 5\ M_\oplus$.

3.2. Discussion

This is backed up by recent studies of disintegrated planet debris in polluted white dwarf spectra (Jura & Young 2014; Xu et al. 2014; Wilson et al. 2015). These studies show that the accreted extrasolar planet debris generally resemble bulk Earth composition (>85% by mass composed of O, Mg, Si, Fe), similar Fe/Si and Mg/Si ratio, and are carbon-poor. This indicates formation processes similar to those controlling the formation and evolution of objects in the inner solar system (Jura & Young 2014).

In our solar system, evidence suggests that rocky bodies were formed from chondritic-like materials (cf. Lodders & Fegley 2010). Current planet formation theory suggests that the solar nebula was initially heated to very high temperatures to the extent that virtually everything was vaporized except for a small amount of presolar grains (Ott 2007). The nebula then cools to condense out various elements and mineral assemblages from the vapor phase at different temperatures according to the condensation sequence (White 2013). Fe–Ni metal alloy and Mg-silicates condense out around similar temperatures of 1200–1400 K (depending on the pressure of the nebula gas) according to thermodynamic condensation calculation (Lodders 2003). Oxygen, on the other hand, does not have a narrow condensation temperature range, as it is very abundant and it readily combines with all kinds of metals to form oxides which condense out at various temperatures as well as H, N, and C to form ices condensing out at relatively low temperatures (Lewis 1997). As supported by the polluted white dwarf study, we expect other exoplanetary systems to follow similar condensation sequence as the solar system in a H-dominated nebular environment for the major elements: Fe, Mg, Si, and O (Jura & Young 2014).

In our solar system, the primitive CI Carbonaceous Chondrites have Fe:Mg:Si = 0.855:1.047:1 (McDonough & Sun 1995). If all this Fe forms the core, the CMF $\approx$ 0.38 is the upper limit. If some Fe is incorporated into the mantle either as metal or oxides, the CMF becomes less. The solar ratio of Fe/Si is representative for the stars in the solar neighborhood, which is a tight distribution centered at 1, while the Mg/Si = 1 seems to tend toward the lower end of the distribution centered at 1.34 (Gilli et al. 2006; Grasset et al. 2009). A Mg/Si ratio higher than 1

could produce more olivine (Mg_2SiO_4) or more MgO to affect the mineralogy of the upper mantle (Bond et al. 2010; Delgado Mena et al. 2010; Pagano et al. 2015). However, it does not affect high-pressure EOS much. As we have pointed out earlier in Section 2 of EOS, the TFD EOS of MgO, SiO_2, $MgSiO_3$, and Mg_2SiO_4 will converge above ~1 TPa due to their identical average atomic weight of 20 and their atomic charge of 10. Therefore, for more massive planets, the effect of Mg/Si tends to be smaller. The dispersion expected from the variation in Mg/Si and Fe/Si ratios cause approximately 2% difference in radius (Grasset et al. 2009; Dressing et al. 2015).

Oxygen is more readily available than Fe, Mg, or Si (Lodders 2003) because it is richly produced in nuclear synthesis of massive stars and the chemical evolution of the Galaxy (Pagel 1997), so there is usually enough O to combine with Mg and Si to form Mg-silicates as well as to oxidize some Fe-metal. If we compare bodies in our solar system, the core mass fractions of Earth and Venus (Rubie et al. 2007, pp. 51–90) are around 0.3, the core mass fraction of Mars is estimated to be 0.2 (McSween 2003), and the core mass fraction of Vesta is smaller, about 0.17 (Ruzicka et al. 1997; Ermakov et al. 2014). The core mass fractions of asteroid parent bodies of iron meteorites are even smaller (Petaev & Jacobsen 2004). As such, there seems to exist a trend of increasing CMFs from smaller objects toward bigger objects in the solar system. This trend seems to turn flat around 1 $M_\oplus$.

These dense exoplanets between 2 and 5 $M_\oplus$ so far appear to agree with the mass–radius relation with a CMF ≈ 0.26, suggesting that they are like the Earth in terms of their proportions of mantle and core. But their surface conditions are utterly different as they are much too hot. This is due to the observational bias that currently it is much easier for us to detect close-in planets around stars. The fact that we now see so many of them suggests there may be abundant Earth-like analogs at proper distances from their stars to allow the existence of liquid water on their surfaces.

4. SUMMARY

This paper provides a new CMF-dependent, semi-empirical mass–radius relation for rocky planets of $0 \leqslant \mathrm{CMF} \leqslant 0.4$ and $1M_\oplus \leqslant M \leqslant 8M_\oplus$.

The result of fit to several dense exoplanets, CMF $\approx 0.26 \pm 0.07$, agrees with the studies of disintegrated planet debris in polluted white dwarf spectra, the solar system formation theory, and the geochemical and cosmochemical evidence of meteorites.

The model tool is accessible at www.astrozeng.com.

The author Li Zeng is grateful to the Simons Foundation for supporting his postdoctoral research position under the Simons Collaboration on the Origins of Life; he would also like to thank Courtney Dressing, Lars Buchhave, and Eugenia Hyung for their inspiring discussions. Part of this research was conducted under the Sandia Z Fundamental Science Program and supported by the Department of Energy National Nuclear Security Administration under award number DE-NA0001804 and DE-NA0002937 to S. B. Jacobsen (PI) with Harvard University. This research is the view of the authors and not those of the DOE.

REFERENCES

Alfè, D., Gillan, M. J., & Price, G. D. 2002, E&PSL, 195, 91
Anderson, W. W., & Ahrens, T. J. 1994, JGR, 99, 4273
Badro, J., Fiquet, G., Guyot, F., et al. 2007, E&PSL, 254, 233
Ballard, S., Huber, D., Chaplin, W., et al. 2014, ApJ, 790, 12
Barros, S. C. C., Almenara, J. M., Deleuil, M., et al. 2014, A&A, 569, A74
Batalha, N. M., Borucki, W. J., Bryson, S. T., et al. 2011, ApJ, 729, 27
Berta-Thompson, Z. K., Irwin, J., Charbonneau, D., et al. 2015, Natur, 527, 204
Bina, C. R. 2003, TrGeo, 2, 39
Birch, F. 1952, JGR, 57, 227
Bond, J. C., O'Brien, D. P., & Lauretta, D. S. 2010, ApJ, 715, 1050
Caracas, R., & Cohen, R. E. 2008, PEPI, 168, 147
Carter, J. A., Agol, E., Chaplin, W. J., et al. 2012, Sci, 337, 556
Charbonneau, D., Berta, Z. K., Irwin, J., et al. 2009, Natur, 462, 891
Cochran, W. D., Fabrycky, D. C., Torres, G., et al. 2011, ApJS, 197, 7
Delgado Mena, E., Israelian, G., González Hernández, J. I., et al. 2010, ApJ, 725, 2349
Dewaele, A., Loubeyre, P., Occelli, F., et al. 2006, PhRvL, 97, 215504
Dragomir, D., Matthews, J. M., Eastman, J. D., et al. 2013, ApJL, 772, L2
Dressing, C. D., Charbonneau, D., Dumusque, X., et al. 2015, ApJ, 800, 135
Dumusque, X., Bonomo, A. S., Haywood, R. D., et al. 2014, ApJ, 789, 154
Dziewonski, A. M., & Anderson, D. L. 1981, PEPI, 25, 297
Ermakov, A. I., Zuber, M. T., Smith, D. E., et al. 2014, Icar, 240, 146
Fischer, R. A., Campbell, A. J., Caracas, R., et al. 2012, E&PSL, 357, 268
Fortney, J., Marley, M., & Barnes, J. 2007, ApJ, 659, 1661
Gilli, G., Israelian, G., Ecuvillon, A., Santos, N. C., & Mayor, M. 2006, A&A, 449, 723
Grasset, O., Schneider, J., & Sotin, C. 2009, ApJ, 693, 722
Hatzes, A. P., Fridlund, M., Nachmani, G., et al. 2011, ApJ, 743, 75
Haywood, R. D., Collier Cameron, A., Queloz, D., et al. 2014, MNRAS, 443, 2517
Huang, H., Fei, Y., Cai, L., et al. 2011, Natur, 479, 513
Jura, M., & Young, E. D. 2014, AREPS, 42, 45
Lewis, J. S. 1997, Physics and Chemistry of the Solar System (Cambridge, MA: Elsevier)
Lodders, K. 2003, ApJ, 591, 1220
Lodders, K., & Fegley, B. 2010, Chemistry of the Solar System (London: Royal Society of Chemistry)
McDonough, W. 2014, in Treatise on Geochemistry, ed. H. D. H. K. Turek (2nd ed.; Oxford: Elsevier)
McDonough, W., & Sun, S. 1995, ChGeo, 120, 223
McSween, H. Y., Jr. 2003, TrGeo, 1, 601
Motalebi, F., Udry, S., Gillon, M., et al. 2015, arXiv:1507.08532
Nelson, B. E., Ford, E. B., Wright, J. T., et al. 2014, MNRAS, 441, 442
Ott, U. 2007, in Presolar Grains in Meteorites and Their Compositions, ed. R. von Steiger, G. Gloeckler, & G. M. Mason (Berlin: Springer Science +Business Media), 87
Pagano, M., Truitt, A., Young, P. A., & Shim, S.-H. 2015, ApJ, 803, 90
Pagel, B. E. J. 2009, Nucleosynthesis and Chemical Evolution of Galaxies (2nd ed.; Cambridge: Cambridge Univ. Press)
Pepe, F., Collier Cameron, A., Latham, D. W., et al. 2013, arXiv:1310.7987
Petaev, M. I., & Jacobsen, S. B. 2004, M&PS, 39, 1685
Poirier, J.-P. 1994, PEPI, 85, 319
Ricolleau, A., Fei, Y., Cottrell, E., et al. 2009, GeoRL, 36, L06302
Ritsema, J., Deuss, A., van Heijst, H. J., & Woodhouse, J. H. 2011, GeoJI, 184, 1223
Rubie, D., Nimmo, F., & Melosh, H. 2007, in Treatise on Geophysics, ed. G. Schubert (Amsterdam: Elsevier)
Ruzicka, A., Snyder, G. A., & Taylor, L. A. 1997, M&PS, 32, 825
Salpeter, E. E., & Zapolsky, H. S. 1967, PhRv, 158, 876
Seager, S., Kuchner, M., Hier-Majumder, C. A., & Militzer, B. 2007, ApJ, 669, 1279
Spera, F. J., Yuen, D. A., & Giles, G. 2006, PEPI, 159, 234
Stacey, F. D., & Davis, P. M. 2008, Physics of the Earth (4th ed.; Cambridge: Cambridge Univ. Press)
Stixrude, L., Wasserman, E., & Cohen, R. E. 1997, JGR, 102, 24729
Umemoto, K., & Wentzcovitch, R. M. 2011, E&PSL, 311, 225
Unterborn, C. T., Dismukes, E. E., & Panero, W. R. 2015, arXiv:1510.07582
Valencia, D., O'Connell, R. J., & Sasselov, D. 2006, Icar, 181, 545
Valencia, D., Sasselov, D. D., & O'Connell, R. J. 2007a, ApJ, 665, 1413
Valencia, D., Sasselov, D. D., & O'Connell, R. J. 2007b, ApJ, 656, 545
Vanderburg, A., Montet, B. T., Johnson, J. A., et al. 2015, ApJ, 800, 59
Wagner, F. W., Tosi, N., Sohl, F., Rauer, H., & Spohn, T. 2012, A&A, 541, A103
White, W. M. 2013, Geochemistry (Hoboken, NJ: Wiley-Blackwell)
Wilson, D. J., Gänsicke, B. T., Koester, D., et al. 2015, MNRAS, 451, 3237
Winn, J. N., Matthews, J. M., Dawson, R. I., et al. 2011, ApJL, 737, L18
Wu, S., Umemoto, K., Ji, M., et al. 2011, PhRvB, 83, 184102
Xu, S., Jura, M., Koester, D., Klein, B., & Zuckerman, B. 2014, ApJ, 783, 79
Zeng, L., & Sasselov, D. 2013, PASP, 125, 227
Zeng, L., & Seager, S. 2008, PASP, 120, 983